

Article

Outage Probability versus Carrier Frequency in GeoSurf Satellite Constellations with Radio-Links Faded by Rain

Emilio Matricciani *  and Carlo Riva 

Dipartimento di Elettronica, Informazione e Bioingegneria, Politecnico di Milano, Piazza L. da Vinci, 32, 20133 Milano, Italy

* Correspondence: emilio.matricciani@polimi.it

Abstract: For sites located in different climatic regions, we estimated the relationship between the annual average probability distribution of exceeding a fixed rain attenuation, and the carrier frequency in the range 16 to 100 GHz, in the zenith paths of GeoSurf satellite constellations. In these constellations rain attenuation is independent of the altitude and number of satellites. Rain attenuation is calculated with the Synthetic Storm Technique, a reliable prediction method, by using on-site measured rain-rate time series. A suitably defined outage probability factor shows that the outage probability, for fixed power margin, tends to saturate as frequency increases. In wideband radio-links, such as in spread spectrum design, there is very likely a long-term distortion due to the in-band outage probability. The results are oriented to design systems faded by rain attenuation whose value is also the total power margin available due to a mixture of coding and hardware technology, whose combination is not of concern here.

Keywords: GeoSurf; in-band outage probability; outage probability; rain attenuation; satellite radio-links; Synthetic Storm Technique; wideband radio-links; zenith path



Citation: Matricciani, E.; Riva, C. Outage Probability versus Carrier Frequency in GeoSurf Satellite Constellations with Radio-Links Faded by Rain. *Telecom* **2022**, *3*, 504–513. <https://doi.org/10.3390/telecom3030027>

Academic Editor: Sotirios K. Goudos

Received: 26 July 2022

Accepted: 16 August 2022

Published: 18 August 2022

Publisher's Note: MDPI stays neutral with regard to jurisdictional claims in published maps and institutional affiliations.



Copyright: © 2022 by the authors. Licensee MDPI, Basel, Switzerland. This article is an open access article distributed under the terms and conditions of the Creative Commons Attribution (CC BY) license (<https://creativecommons.org/licenses/by/4.0/>).

1. The GeoSurf Satellite Constellations

The GeoSurf satellite constellations belong to the family of Walker Star Constellations and they emulate, for ground stations located at any latitude, the geostationary orbit with zenith paths: Any transmitter/receiver, wherever located, can be linked to a satellite as if it were at the equator and the satellite at its zenith [1]. The GeoSurf constellations can have most of the advantages of the current GEO (Geostationary), MEO (Medium Earth Orbit), and LEO (Low Earth Orbit) satellite constellations without having most of their drawbacks. Table 1 of ref. [1] compares the advantages and disadvantages of GeoSurf constellations with GEO, MEO and LEO constellations. Ref. [2] compared the tropospheric attenuation of GeoSurf satellite paths with those of GEO, MEO, and LEO satellites.

Compared with ref. [2], in this paper we consider only the zenith paths of the GeoSurf constellation and rain attenuation only, without any further comparison with the GEO, MEO, and LEO radio-links. In fact, our aim is to estimate the relationship between the annual average probability distribution $P(A)$ of exceeding a given rain attenuation A (dB) and the carrier frequency f (GHz)—i.e., the center frequency of bandwidth B_w —beyond 16 GHz in the GeoSurf paths (local zenith paths). The satellite radio-link can be modeled as an additive white Gaussian noise channel in which the in-band frequencies can be attenuated differently by rain attenuation when the bandwidth is significantly large, i.e., of the order of at least 1 GHz (wideband modulation).

Our results are oriented to system design. If the constellation radio-links have a fixed signal-to-noise power margin, and this margin is attributed only to rain attenuation A , then $P(A)$ is also the outage probability of the radio-links. Because we wish to show system-oriented results, we limited the power margin/attenuation in the range 3 to 30 dBs and the frequency range between 16 GHz and 100 GHz. In other words, we considered

rain attenuation $3 \leq A \leq 30$ dBs and carrier frequency $16 \leq f \leq 100$ GHz and studied how $P(A)$ changes for a fixed value of A . However, we anticipate that the results can be applied also to larger rain attenuation because the modelling of a suitable defined outage probability factor is insensitive to rain attenuation, as shown below.

Table 1. Geographical coordinates, altitude (km), rain height H_R (km), and number of years of continuous rain rate measurements at the indicated sites.

Site	Latitude N (°)	Longitude E (°)	Altitude H_S (km)	Precipitation Height H_R (km)	Rain Rate Data Bank (Years)
Spino d'Adda (Italy)	45.4	9.5	0.084	3.341	8
Gera Lario (Italy)	46.2	9.4	0.210	3.483	5
Fucino (Italy)	42.0	13.6	0.680	2.905	5
Madrid (Spain)	40.4	356.3	0.630	3.001	8
Prague (Czech Republic)	50.0	14.5	0.250	3.051	5
Tampa (Florida)	28.1	277.6	0.050	4.528	4
Norman (Oklahoma)	35.2	262.6	0.420	4.145	4
White Sands (New Mexico)	32.5	253.4	1463	4.744	5

Notice that, in our study, it does not matter how the power margin of a radio-link is obtained: it can be a combination of coding and hardware, which can vary very rapidly as technology develops. What counts is the total value, which is here supposed to compensate for rain attenuation.

For illustrating the general characteristics of the relationship $P(A)$ versus f , we report the results concerning the sites listed in Table 1, located in different climatic regions. The rain attenuation expected in GeoSurf radio-links is independent of the particular GeoSurf design (e.g., altitude and number of satellites), because all paths to/from a satellite of the constellation are always vertical (zenith). A was calculated with the Synthetic Storm Technique (SST) [3]. We considered these specific sites because of the availability of the rain-rate time series $R(t)$ (mm/h), with rain rate averaged in 1 min intervals, continuously recorded on-site for several years, although in zenith paths the SST requires only to know the probability distribution of rain rate $P(R)$ (see Equation (29) of ref. [3]). In other words, calculations and models reported below can be derived for any site where on-site measured—best choice—or estimated $P(R)$ is available.

Since the 1960's, many experiments and studies have been conducted—and reported in a huge numbers of papers—to establish the impact of rain attenuation on the outage probability of fixed (i.e., GEO) and mobile satellite (i.e., MEO and LEO) communications. Because of the saturation of the lower frequency bands currently used, as hardware and transmitter performance improves, satellite communication systems tend to use higher frequencies and larger bandwidths, including THz frequencies [4], for GEO, MEO, and LEO constellations. Unfortunately, rain attenuation, besides clear-sky fading, is still the most serious physical and unavoidable source of outage; therefore, studies, as the one reported in the present paper, or in ref. [5], are always welcome.

After this introductory section, Section 2 reports and discusses the probability distributions of rain attenuation at the reference sites in zenith paths obtained with the SST, Section 3 defines and reports a suitable outage probability factor at the reference sites, Section 4 models the outage probability factor, Section 5 defines the in-band outage probability factor, and finally Section 6 concludes.

2. The Synthetic Storm Technique Applied to Zenith Paths

Satellite communication links at centimeter and millimeter wave frequencies are faded by rainfall. For a reliable link-budget design, we need to know, at the very least, the annual probability distribution function, $P(A)$, of rain attenuation A (dB) measured/predicted in the up- or down-links to a satellite. Instead of long and expensive measurements of beacon attenuation, prediction models are used for estimating $P(A)$ from locally, measured or

estimated, annual probability distributions, $P(R)$, of 1 min rain rate R . The Synthetic Storm Technique [3] is a powerful and accurate tool, as is now recognized, that can produce all the necessary statistics of rain attenuation, not only $P(A)$, but also fade durations and rate of change of attenuation because it provides reliable rain attenuation time series $A(t)$. From knowing the rain-rate time series $R(t)$ (mm/h, averaged in 1 min intervals), recorded at a site, the SST can generate $A(t)$, at any frequency and polarization, and for any slant path above about 10° . Because it reproduces reliable $A(t)$, it has been used in the last 30 years for many purposes by several researchers [6–20].

When the Synthetic Storm Technique is applied to zenith paths, the rain attenuation time series lasts exactly as the rain-rate time series, as discussed in ref. [3], Equations (18) and (29).

The vertical (zenith) structure of precipitation is modeled with two layers of precipitation of different depths, a model taken from ref. [21]. Starting from the ground, there is rain (hydrometeors in the form of raindrops, water temperature of 20°C , called layer A), followed by a melting layer, i.e., melting hydrometeors at 0°C , layer B. The vertical rain rate R (mm/h, averaged in 1 min) in layer A is assumed to be uniform and given by that measured at ground, i.e., by the rain gauge, $R_A = R$. By assuming simple physical hypotheses, calculations showed that the vertical precipitation rate in the melting layer, termed “apparent rain rate”, is also uniform and given by $R_B = 3.134 \times R_A$ [21]. The height of the precipitation (rain and melting layer, H_R) above sea level to be used in the simulation is the latest estimate of the ITU-R [22]. The layer B depth is 0.40 km, regardless of the latitude [3,21].

Now, according to Equation (29) of ref. [3], rain attenuation $A(t)$ (dB) in the zenith path is given by:

$$A(t) = k_A R(t)^{\alpha_A} \times (H_R - 0.4 - H_s) + k_B (3.134 \times R(t))^{\alpha_B} \times 0.4 \tag{1}$$

In Equation (1), k and α are the constants that give the specific rain attenuation $Y = kR^\alpha$ — R measured in mm/h and Y in dB per 1 km—in the two layers from the rain rate R measured at the ground, calculated at 20°C in layer A and at 0°C in layer B [3], values given in ref. [23].

Finally, because the relationship between $A(t)$ and $R(t)$ is monotonic, the on-site probability distribution $P(R)$ is transformed directly into the $P(A)$ of the zenith path through the variable transformation given by Equation (1).

Figures 1–4 show examples of the $P(A)$ obtained at several frequencies at the sites listed in Table 1. Because our analysis is oriented to find the outage probability when the radio-link power margin is not larger than A dB, $P(A)$ is also the radio-link outage probability due to rain.

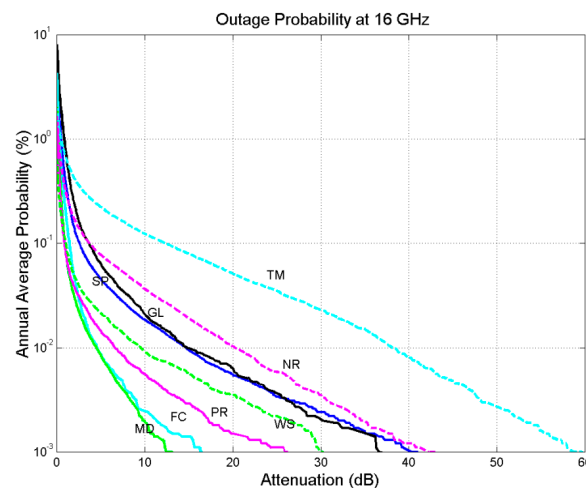


Figure 1. Annual average probability $P(A)$ (%) of exceeding the rain attenuation A (dB) indicated in abscissa, at the indicated sites: Spino d’Adda (SP, blue continuous line); Gera Lario (GL, black continuous

line); Fucino (FC, cyan continuous line); Madrid (MD, green continuous line); Prague (PR, magenta continuous line); Tampa (TM, cyan dashed line); Norman (NR, magenta dashed line); White Sands (WS, green dashed line), at 16 GHz in zenith paths. When the power margin in the zenith radio-links of the GeoSurf satellite constellations is equal to A (dB), $P(A)$ represents the outage probability.

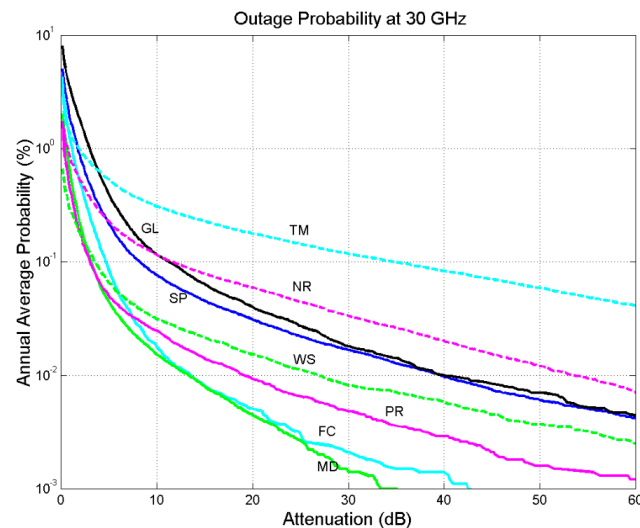


Figure 2. Annual average probability $P(A)$ (%) of exceeding the rain attenuation A (dB) indicated in abscissa, at the indicated sites: Spino d'Adda (SP, blue continuous line); Gera Lario (GL, black continuous line); Fucino (FC, cyan continuous line); Madrid (MD, green continuous line); Prague (PR, magenta continuous line); Tampa (TM, cyan dashed line); Norman (NR, magenta dashed line); White Sands (WS, green dashed line), at 30 GHz in zenith paths. When the power margin in the zenith radio-links of the GeoSurf satellite constellations is equal to A (dB), $P(A)$ represents the outage probability.

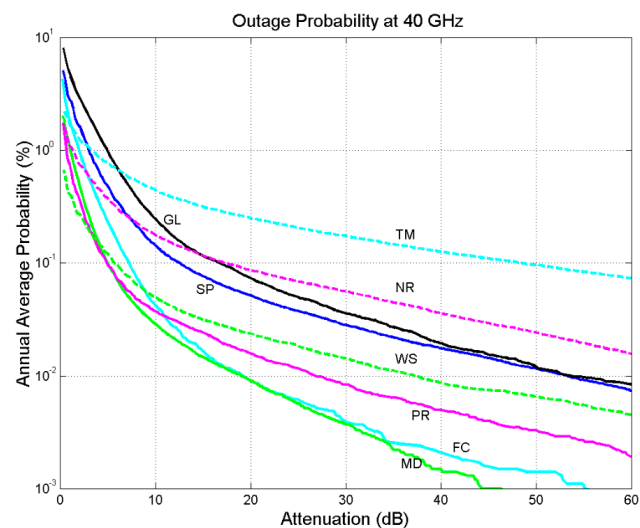


Figure 3. Annual average probability $P(A)$ (%) of exceeding the rain attenuation A (dB) indicated in abscissa, at the indicated sites: Spino d'Adda (SP, blue continuous line); Gera Lario (GL, black continuous line); Fucino (FC, cyan continuous line); Madrid (MD, green continuous line); Prague (PR, magenta continuous line); Tampa (TM, cyan dashed line); Norman (NR, magenta dashed line); White Sands (WS, green dashed line), at 40 GHz in zenith paths. When the power margin in the zenith radio-links of the GeoSurf satellite constellations is equal to A (dB), $P(A)$ represents the outage probability.

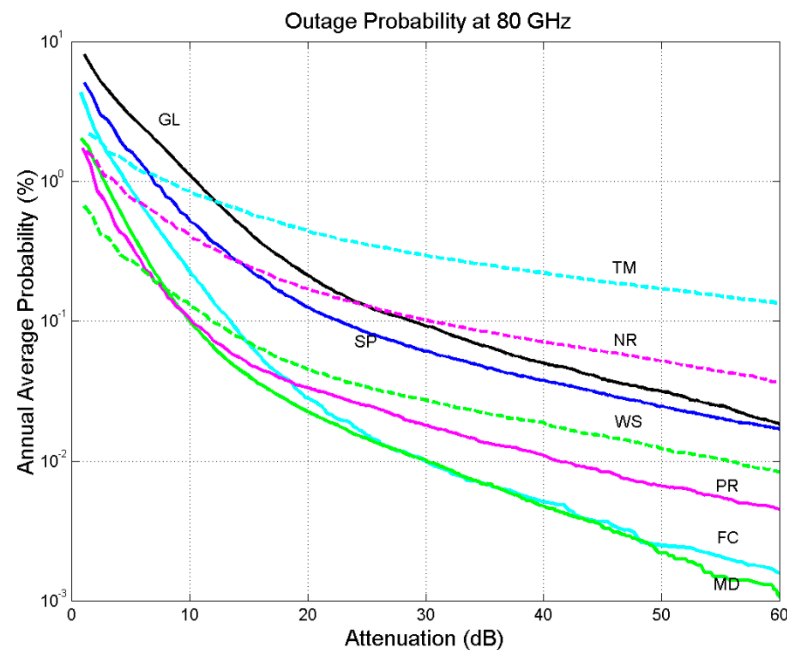


Figure 4. Annual average probability $P(A)$ (%) of exceeding the rain attenuation A (dB) indicated in abscissa, at the indicated sites: Spino d’Adda (SP, blue continuous line); Gera Lario (GL, black continuous line); Fucino (FC, cyan continuous line); Madrid (MD, green continuous line); Prague (PR, magenta continuous line); Tampa (TM, cyan dashed line); Norman (NR, magenta dashed line); White Sands (WS, green dashed line), at 80 GHz in zenith paths. When the power margin in the zenith radio-links of the GeoSurf satellite constellations is equal to A (dB), $P(A)$ represents the outage probability.

In the next section, we show how $P(A)$ changes as the frequency increases from 16 to 100 GHz, for a fixed power margin A , by defining a suitable outage probability factor.

3. Outage Probability Factor

We modeled the relationship between the outage probability $P(A)$ due to rain attenuation A as follows. For a site, let us consider a fixed value A for all frequencies and start by considering, as reference value, the probability $P_{f_0}(A)$ exceeded at a reference frequency f_0 , 16 GHz in our modelling. The reference $P(A)$, for a given A , is therefore that shown in Figure 1 for each site.

We can relate $P(A)$ exceeded at frequencies $f \geq 16$ GHz to the reference probability exceeded at 16 GHz, by writing:

$$P(A, f) = P(A, f_0)\rho(A, f) \quad (2)$$

Now, as $f \geq f_0$ it follows that the probability factor $\rho(A, f) \geq 1$ because the same attenuation is exceeded at frequency $f > f_0$ with a larger probability.

Figures 5 and 6 show how $\rho(A, f)$ changes as a function of frequency, for fixed values of A ranging approximately from 3 to about 30 dB in 0.2 dB steps, for some sites. Each curve shown in Figures 5 and 6 corresponds, of course, to a fixed value A . The red curve shows the average values $\rho_m(f)$, a parameter independent, of course, of attenuation.

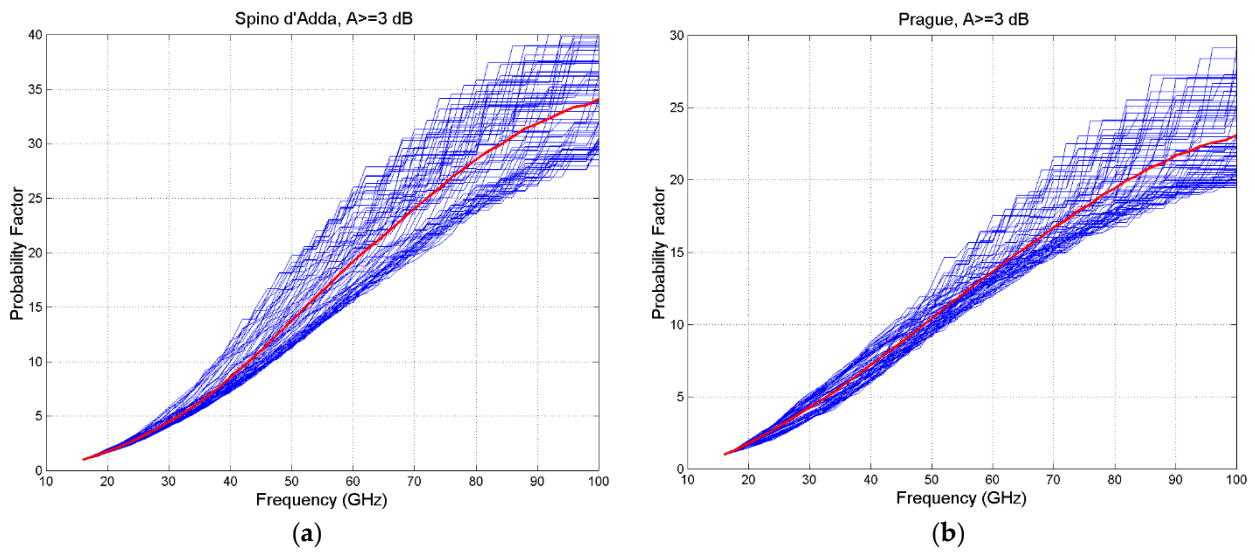


Figure 5. Probability factor $\rho(A, f)$ as function of frequency, for fixed values of A ranging approximately from 3 to about 30 dB in 0.2 dB steps (blue continuous curves): (a) for Spino d'Adda; (b) Prague. The red curve is the average value $\rho_m(f)$, a parameter independent of attenuation. Notice the different ordinate range.

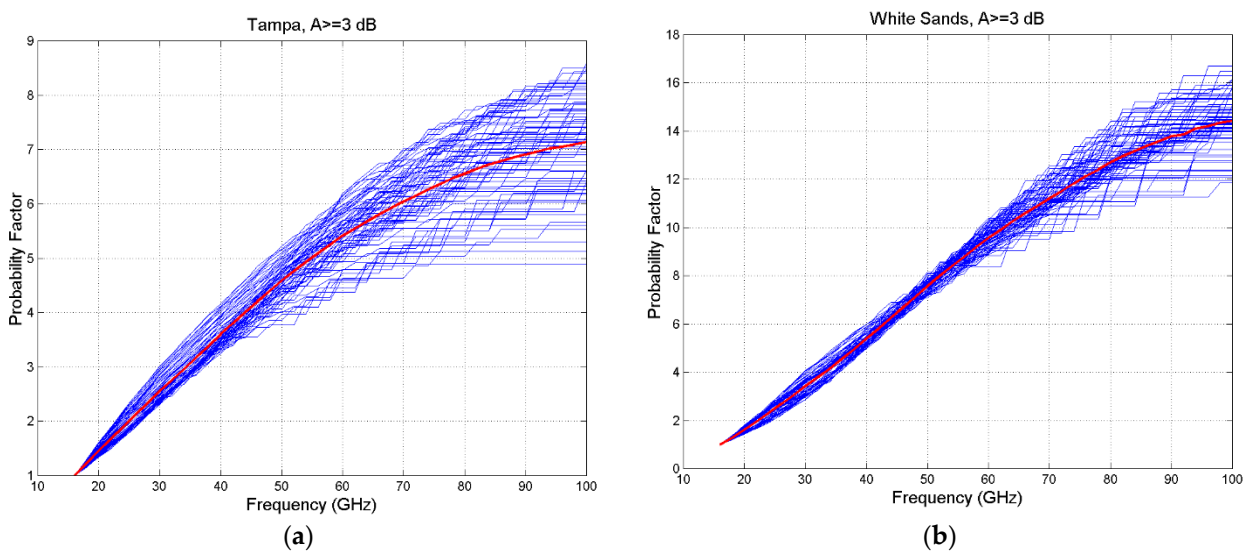


Figure 6. Probability factor $\rho(A, f)$ as function of frequency, for fixed values of A ranging approximately from 3 to about 30 dB in 0.2 dB steps (blue continuous curves): (a) Tampa; (b) White Sands. The red curve is the average value $\rho_m(f)$, a parameter independent of attenuation. Notice the different ordinate range.

Because of the different climatic rainfall regions, each site shows quite different values. However—as the average values (red curves) show—as frequency increases, the curves tend to saturate. The saturation values depend on the site considered, but this occurs approximately at about 100 GHz. Notice, however, that the spread of the curves shown in Figures 5 and 6 is not very large, therefore indicating a small sensitivity to the maximum value (30 dBs) of the rain attenuation considered.

In conclusion, if a radio-link has a fixed power margin A , as assumed in Figures 5 and 6, as the carrier frequency increases the outage probability also increases across a large bandwidth centered on the carrier frequency f , as next section shows.

4. Model of the Average Outage Probability Factor

The average outage probability factor $\rho_m(f)$ shown in Figures 5 and 6, by setting $f_o = 16$ GHz, can be modeled (best-fit analysis) with the following mathematical expression:

$$\rho_m(f) = 1 + (f - f_o)^a - (f - f_o)^b \quad (3)$$

Notice that each addend in the right-hand side of Equation (3) has no particular physical meaning; what counts is the sum of the addends. The constants a and b are reported in Table 2, for each site. For Spino d'Adda, as example, for $A = 3$ dB, $P_{16 \text{ GHz}}(3) = 0.081\%$ (Figure 1), now at 40 GHz the average probability factor, from (3) and Table 2, turns out to be $\rho_m = 9.70$; therefore, the estimated $P_{40 \text{ GHz}}(3) = 0.787\%$ (outage time about 70 h in an average year) is to be compared to $P_{40 \text{ GHz}}(3) = 0.954\%$ (Figure 3).

Table 2. Constants a and b of Equation (3) for the indicated sites.

Site	a	b
Spino d'Adda (Italy)	0.937	0.753
Gera Lario (Italy)	1.008	0.756
Fucino (Italy)	1.123	0.823
Madrid (Spain)	1.007	0.518
Prague (Czech Republic)	0.828	0.623
Tampa (Florida)	0.532	0.315
Norman (Oklahoma)	0.655	0.411
White Sands (New Mexico)	0.711	0.495

In Table 2, notice that when the climatic rainfall regions are very similar, as is the case for Spino d'Adda and Gera Lario, the curves tend to coincide.

Let us assess how good the best-fit given by Equation (3) is by studying the error it gives in considering only the carrier frequency as independent variable. We defined the error as follows (%):

$$\varepsilon = 100 \times \frac{\rho_m(f) - \rho(A, f)}{\rho(A, f)} \quad (4)$$

Figure 7 shows the mean error versus frequency. In general, the error is very low, for this kind of measurement, not exceeding $\pm 30\%$. Notice, however, that the purpose of the modelling (3) is not to predict the result—obviously all data shown in Figures 5 and 6 are available—but to show the general trend.

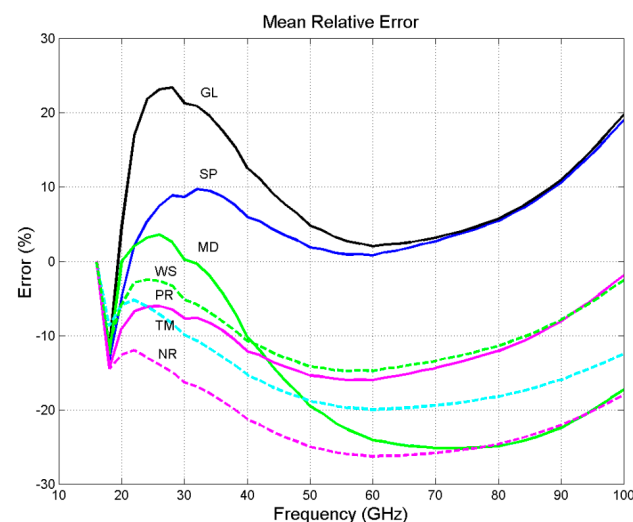


Figure 7. Mean error (%) produced by Equation (3) as frequency increases from 16 GHz to 100 GHz. Spino d'Adda (SP, blue continuous line); Gera Lario (GL, black continuous line); Madrid (MD, green

continuous line); Prague (PR, magenta continuous line); Tampa (TM, cyan dashed line); Norman (NR, magenta dashed line); White Sands (WS, green dashed line).

New satellite radio-links—such as those with spread-spectrum design—may occupy a large radiofrequency bandwidth centered at frequency f_c , in which, for a fixed power margin, it is very likely to find different equivalent outages at the extremes of the bandwidth, which may produce signal distortions. In the next section we discuss this issue.

5. In-Band Outage Probability Factor

If large-bandwidth (wideband) radio-links are designed, such those in satellite communications with spread spectrum or similar methods, we should know how much the outage probability changes within the large bandwidth, for a fixed power margin A , to assess possible signal linear distortions.

We can estimate the change expected in the bandwidth by studying the in-band probability factor I_p (GHz^{-1}) defined as:

$$I_p = [(d\rho_m(f))/df]/(\rho_m(f)) \quad (5)$$

In Equation (5), $d\rho_m(f)/df$ is the frequency derivative of Equation (3) and $\rho_m(f)$ is given by Equation (3). To estimate from Equation (5) the value of I_p in a bandwidth B_w (GHz) centered in $f = f_c$ it is sufficient to multiply the right-hand side approximately for B_w ; therefore, Equation (4) numerically refers to $B_w = 1$ GHz, hence, in finite terms it gives the ratio $I_p = \Delta\rho_m(f_c)/\rho_m(f_c)$ in the 1-GHz bandwidth around f_c . Therefore, at the frequency $f = f_c + 0.5$ GHz the outage is greater because the same rain attenuation is exceeded with higher probability than at the lower frequency $f = f_c - 0.5$ GHz. In other words, to avoid outage in all bandwidth, the power margin must be equal to the rain attenuation measured at $f = f_c + 0.5$ GHz, not at $f = f_c$.

Figure 8 shows I_p for the indicated sites. It is evident that the distortion due to the different in-band outage probability—because of a fixed power margin in the AWGN channel calculated at $f = f_c$ —can be significantly different from site to site, and also at a site from frequency to frequency. For Spino d’Adda, at $f = 40$ GHz, continuing the example of Section 3, $I_p = 0.044$; therefore, the outage time difference between the extreme frequencies in $B_w = 1$ GHz bandwidth is $(0.044) \times 70 = 3.1$ hours in an average year. To a first approximation, this time difference is proportional to B_w .

In general, higher frequencies show lower values because a fixed rain attenuation is exceeded with very near probabilities than at lower frequencies. This is evident for Tampa (see Figures 1–4), which gives the lowest curve in Figure 8. The opposite behavior is found when the fixed rain attenuation at higher frequencies is exceeded with different probability than at lower frequencies, as it occurs for Madrid (see Figures 1–4), which gives the highest values in Figure 8. In other words, the slopes of the probability distribution, as those shown in Figures 1–4—i.e., the probability density function of rain attenuation and, in the zenith paths here considered, also of rain rate—affect this kind of distortion more than other parameters.

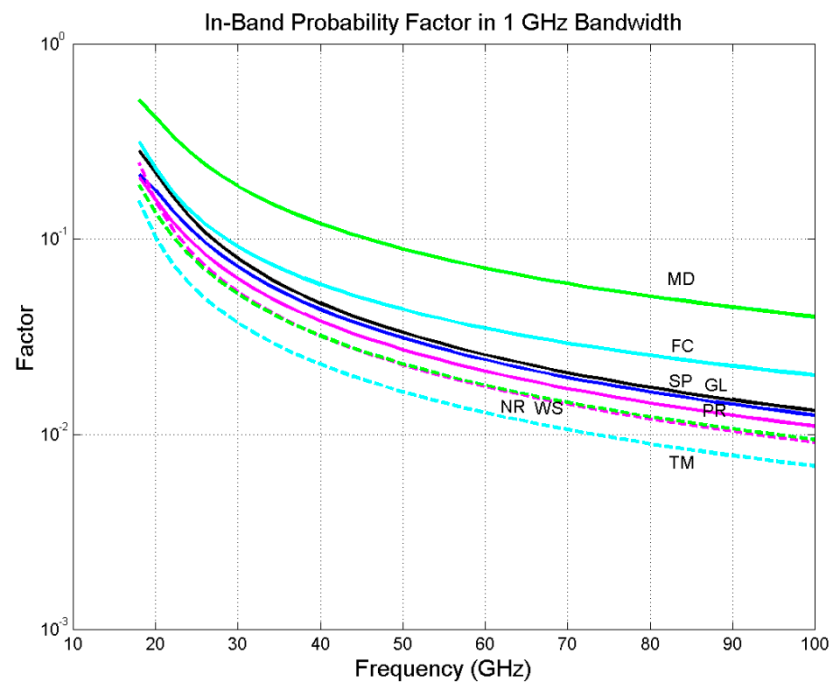


Figure 8. In-band probability factor I_p , Equation (4), versus frequency, Equation (5), at the indicated sites for $B_w = 1$ GHz: Spino d’Adda (SP, blue continuous line); Gera Lario (GL, black continuous line); Fucino (FC, cyan continuous line); Madrid (MD, green continuous line); Prague (PR, magenta continuous line); Tampa (TM, cyan dashed line); Norman (NR, magenta dashed line); White Sands (WS, green dashed line), in zenith paths.

6. Conclusions

We estimated the relationship between the annual average probability distribution $P(A)$ of exceeding a given rain attenuation A (dB) and the carrier frequency f (GHz) in the range 16 to 100 GHz, in the zenith paths of GeoSurf satellite constellations and reported results oriented to system design. For illustrating the general characteristics of this relationship, we have reported the results concerning sites located in different climatic regions. The rain attenuation expected in GeoSurf radio-links is independent of the particular GeoSurf design (e.g., altitude and number of satellites), and was calculated with the Synthetic Storm Technique.

We modeled the relationship according to Equations (2) and (3) by defining a suitable outage probability factor. The mean error of the outage probability factor, Equation (4), depends on site. The main result was that this factor tends to saturate at about 100 GHz, therefore giving about the same outage probability, for a fixed attenuation/power margin, as frequency increases. For a fixed power margin, in wideband radio-links, there is very likely a linear distortion due to in-band outage probability.

Further work should be conducted to apply these concepts to very large bandwidth radio-links, such as those envisaged with spread-spectrum techniques, by making more detailed predictions within the large bandwidth with the SST, as discussed above, especially with the purpose of establishing the main features of the radiofrequency transfer function.

Author Contributions: Both authors have equally developed the software, modeled the results and written the paper. All authors have read and agreed to the published version of the manuscript.

Funding: This research received no external funding.

Institutional Review Board Statement: Not applicable.

Informed Consent Statement: Not applicable.

Data Availability Statement: Data and software are available from the authors, on request.

Acknowledgments: We wish to thank our colleagues: Roberto Acosta, researcher at NASA some years ago, for providing the rain rate data of the North America sites; Ondrej Fiser, Institute of Atmospheric Physics in Prague, for providing the rain rate data of Prague; José Manuel Riera, Universidad Politécnica de Madrid, for providing the rain rate data of Madrid.

Conflicts of Interest: The authors declare no conflict of interest.

References

1. Matricciani, E. Geocentric Spherical Surfaces Emulating the Geostationary Orbit at Any Latitude with Zenith Links. *Future Internet* **2020**, *12*, 16. [[CrossRef](#)]
2. Matricciani, E.; Riva, C.; Luini, L. Tropospheric Attenuation in GeoSurf Satellite Constellations. *Remote Sens.* **2021**, *13*, 5180. [[CrossRef](#)]
3. Matricciani, E. Physical-mathematical model of the dynamics of rain attenuation based on rain rate time series and a two-layer vertical structure of precipitation. *Radio Sci.* **1996**, *31*, 281–295. [[CrossRef](#)]
4. Norouzian, F.; Marchetti, E.; Gashinova, M.; Hoare, E.; Constantinou, C.; Gardner, P.; Cherniakov, M. Rain Attenuation at Millimeter Wave and Low-THz Frequencies. *IEEE Trans. Antennas Propag.* **2020**, *68*, 421–431. [[CrossRef](#)]
5. Ning, Q.; Yang, X.; Chen, B.; Zhou, X. The performance analysis of NOMA in LEO satellite rain attenuation and fading hybrid channel. *Int. J. Satell. Commun. Netw.* **2022**, *40*, 256–267. [[CrossRef](#)]
6. Matricciani, E.; Riva, C. The search for the most reliable long-term rain attenuation cdf of a slant path and the impact on pre-diction models. *IEEE Trans. Antennas Propag.* **2005**, *53*, 3075–3079. [[CrossRef](#)]
7. Matricciani, E. Physical-mathematical model of dynamics of rain attenuation with application to power spectrum. *Electron. Lett.* **1994**, *30*, 522–524. [[CrossRef](#)]
8. Matricciani, E. Prediction of fade durations due to rain in satellite communication systems. *Radio Sci.* **1997**, *32*, 935–941. [[CrossRef](#)]
9. Kanellopoulos, S.; Panagopoulos, A.; Matricciani, E.; Kanellopoulos, J. Annual and Diurnal Slant Path Rain Attenuation Statistics in Athens Obtained With the Synthetic Storm Technique. *IEEE Trans. Antennas Propag.* **2006**, *54*, 2357–2364. [[CrossRef](#)]
10. Matricciani, E.; Riva, C.; Castanet, L. Performance of the Synthetic Storm Technique in a Low Elevation 5° Slant Path at 44.5 GHz in the French Pyrénées. In Proceedings of the EuCAP 2006, Nice, France, 6–10 November 2006.
11. Sánchez-Lago, I.; Fontán, F.P.; Mariño, P.; Fiebig, U.C. Validation of the Synthetic Storm Technique as Part of a Time—Series Generator for Satellite Links. *IEEE Antennas Wirel. Propag. Lett.* **2007**, *6*, 372–375. [[CrossRef](#)]
12. Mahmudah, H.; Wijayanti, A.; Mauludiyanto, A.; Hendratoro, G.; Matsushima, A. Analysis of Tropical Attenuation Statistics using Synthetic Storm for Millimeter—Wave Wireless Network Design. In Proceedings of the 5th IFIP International Conference on Wireless and Optical Communications Networks (WOCN '08), Surabaya, Indonesia, 5–7 May 2008.
13. Matricciani, E. A Relationship between Phase Delay and Attenuation Due to Rain and Its Applications to Satellite and Deep—Space Tracking. *IEEE Trans. Antennas Propag.* **2009**, *57*, 3602–3611. [[CrossRef](#)]
14. Matricciani, E. Space communications with variable elevation angle faded by rain: Radio links to the Sun—Earth first Lagrangian point L1. *Int. J. Satell. Commun. Netw.* **2016**, *34*, 809–831. [[CrossRef](#)]
15. Lyras, N.K.; Kourogorgas, C.I.; Panagopoulos, A.D.; Ventouras, S. Rain Attenuation Statistics at Ka and Q band in Athens using SST and Short Scale Dynamic Diversity Gain Evaluation. In Proceedings of the 2016 Loughborough Antennas & Propagation Conference (LAPC), Loughborough, UK, 14–15 November 2016.
16. Matricciani, E. Probability distributions of rain attenuation obtainable with linear combining techniques in space-to-Earth links using time diversity. *Int. J. Satell. Commun. Netw.* **2017**, *36*, 220–237. [[CrossRef](#)]
17. Nandi, A. Prediction of Rain Attenuation Statistics from Measured Rain Rate Statistics using Synthetic Storm Technique for Micro and Millimeter Wave Communication Systems. In Proceedings of the 2018 IEEE MTT-S International Microwave and RF Conference (IMaRC), Kolkata, India, 28–30 November 2018.
18. Jong, S.L.; Riva, C.; D'Amico, M.; Lam, H.Y.; Yunus, M.M.; Din, J. Performance of synthetic storm technique in estimating fade dynamics in equatorial Malaysia. *Int. J. Satell. Commun. Netw.* **2018**, *36*, 416–426. [[CrossRef](#)]
19. Papafragkakis, A.Z.; Kourogorgas, C.I.; Panagopoulos, A.D. Performance Evaluation of Ka- and Q-band Earth-Space Diversity Systems in Attica, Greece using the Synthetic Storm Technique. In Proceedings of the 13th European Conference on Antennas and Propagation (EuCAP 2019), Krakow, Poland, 31 March–5 April 2019.
20. Das, D.; Animesh Maitra, A. Application of Synthetic Storm Technique to Predict Time Series of Rain Attenuation from Rain Rate Measurement for a Tropical Location. In Proceedings of the 5th International Conference on Computers and Devices for Communication (CODEC), Kolkata, India, 17–19 December 2021.
21. Matricciani, E. Rain attenuation predicted with a two-layer rain model. *Eur. Trans. Telecommun.* **1991**, *2*, 715–727. [[CrossRef](#)]
22. *Recommendation ITU-R P.839-4*; Rain height Model for Prediction Methods; ITU: Geneva, Switzerland, 2013.
23. Maggiori, D. Computed transmission through rain in the 1–400 GHz frequency range for spherical and elliptical drops and any polarization. *Alta Freq.* **1981**, *50*, 262–273.